A CHARACTERIZATION OF SAR IMAGES IN THE 2009 L'AQUILA ITALY EARTHQUAKE

Pralhad Uprety

PhD Student
Chiba University
Chiba, Japan

Fumio Yamazaki

Professor
Chiba University
Chiba, Japan

Abstract

Natural disasters have been hitting hard to the different parts of world creating a miserable situations. In the past time, it was often difficult to know the level of disaster damage to the concerned authority because of quick inaccessibility to place or lack of reliable data. However, with the advancement of the remote sensing technology the situation has greatly improved. Remote sensing has become an indispensable tool in the disaster management. Currently, it has been possible to get the high-resolution satellite images after the disaster occurs.

An earthquake rocked the region of Abruzzo in central Italy on April 6, 2009. The epicenter was near the L'Aquila and hence the earthquake is commonly known as the 2009 L'Aquila earthquake. L'Aquila, the capital of Abruzzo, and surrounding villages suffered most damage. 307 people died making this the deadliest earthquake to hit Italy since the 1980 Irpinia earthquake. The earthquake caused injury to more than 1,500 people and made about 65,000 people homeless. This study carries out the building damage detection using the high-resolution SAR imagery.

Keywords: The 2009 L'Aquila Earthquake, SAR imagery, Damage detection

1. Introduction

Disasters are untimely event and often causing widespread damage to lives and property. The more wider definition states disaster as a serious disruption of a community or a society causing widespread human, material, economic and environmental losses which exceed the ability of the community or society to cope using its own level of the resources [1].

The importance of timely action in disaster situation is of utmost importance. Remote sensing especially satellite remote sensing can help a lot by providing the data of large region of affected areas without being there physically. Remote sensing is the science of obtaining information about an object, area or phenomenon through the analysis of data acquired by a device that is not in contact with the object, area or phenomenon under investigation [2]. Broadly, satellite system employs either optical or microwave sensors. Optical sensors are affected by the local weather condition whereas radar system like synthetic aperture radar (SAR) is free from this constrain. SAR image is obtained from the coherent image system [3] and is extraordinary for its capability of the recording the surface condition of the target regardless of weather or the solar illumination. Because of this characteristics SAR is a powerful tool and has been utilized in the disaster situations including earthquakes, wildfire and so on [4]. In this paper, we analyze the damaged buildings of the L'Aquila city center in Italy using high-resolution SAR images.

2. The 2009 L'Aquila Earthquake

Italy (Fig. 1) in general and L'Aquila area in particular had been severely affected by numerous earthquakes in the past. Notable past earthquakes include that of 1315, 1349, 1461, 1703, 1706, 1915, and 1958 [5]. An earthquake of magnitude 5.8 on the Richter scale (6.3 on moment magnitude scale) hit the Central Aburruzo region of Italy on 6th April, 2009 at 3.32 am local time

affecting many human settlements throughout the region. The depth of earthquake was 8.8 kilometer. Figure 2 shows shake map [6] of the earthquake-affected region. This earthquake severely affected old city of L'Aquila. Three hundred seven people died, more than 1,500 people injured and about 65,000 people had been made homeless. Many important structures including San Salvatore Hospital, which was the crucial hospital system in L'Aquila area, had to be evacuated due to the high damage level [7]. It was the deadliest earthquake in Italy after Irpinia earthquake in 1980. This article describes the use of the high-resolution radar satellite images in earthquake damage detection in urban areas of L'Aquila.

Fig. 1: Map of Italy

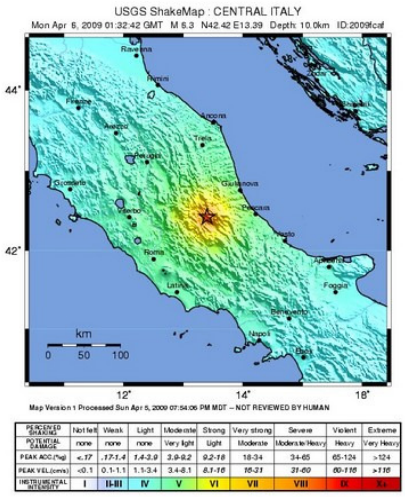

Fig. 2: Shake map of L'Aquila area

2.1 The 2009 L'Aquila earthquake and SAR data

Data employed in this research is from the TerraSAR-X (X- band) satellite system. This X-band data has the wavelength of 3.1 centimeter with the frequency of 9.6 Gigahertz. Data include one pre-seismic data (Feb 6, 2009) and other post-seismic (April 13, 2009) as shown in Fig. 3. Acquisition mode of these data is strip with polarization HH (single). Incidence angle is 39.2 degree. The path of satellite is ascending with right look. These images have spatial resolution of 1.25 meter. The employed data was standard product (2A) and it was radiometrically corrected, sensor corrected, geometrically corrected and mapped to a cartographic projection by the data provider.

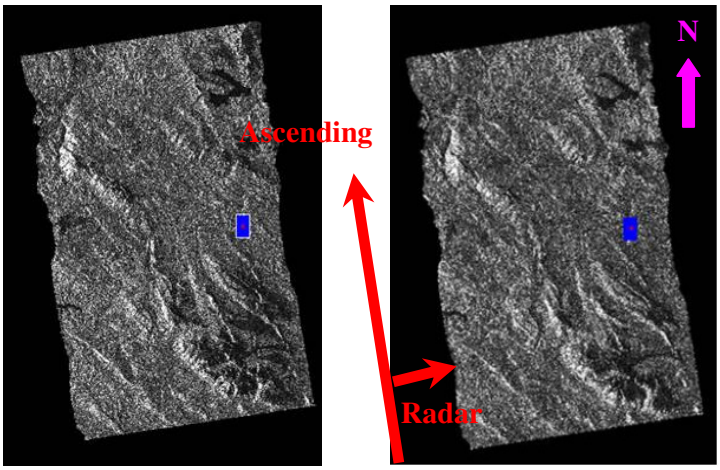

Before Feb 6, 2009 After April 13, 2009

Fig. 3: SAR data of L'Aquila area (the blue portion is the area of concern)

2.2 Basic principles of SAR

SAR is an active sensor as it illuminates the target with its own energy and then records a portion of an energy reflected back to it (commonly called backscatter). Wavelength is normally in the range of 1 cm to 1 m corresponding to a frequency of 30 GHz to 300 MHz. SAR creates comparatively high ground (pixel) resolution as it simulates a long antenna by combining electrical signals received by its sensor as it moves along a particular track. Each pixel in intensity (amplitude) images corresponds to the radar back scattering from the target. Backscattering coefficient is dependent upon the local incidence angle of microwave, electrical characteristics, surface roughness, moisture content of the target and wavelength of the microwave. Man-made structures like metal bridges or buildings typically show much corner reflection also popularly called the cardinal effect. Because of the scattered reflection, open surface or damaged buildings have low backscatter reflectance. Figure 4 shows a schematic diagram of the surface objects and their backscattering properties. The corner reflection of the buildings depends on the height and the aspect angle [6]. Aspect angle refers to the orientation of the building relative to the viewing direction of radar. The backscattering coefficients obtained from pre and post events SAR images, can be used for change/damage detection [4], [9-12].

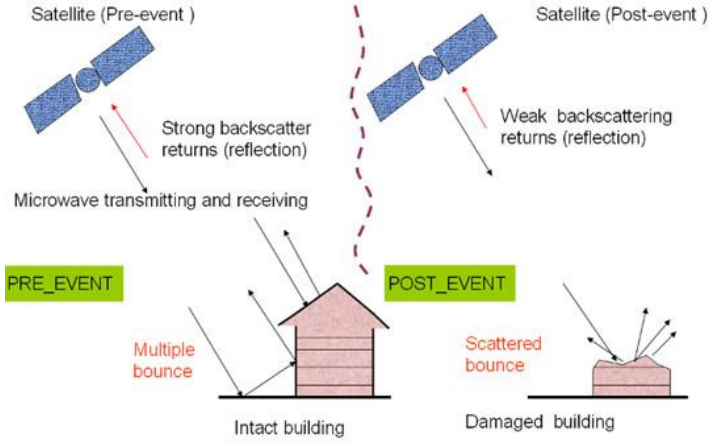

Fig. 4: Schematic figure of the geometry of repeat pass satellite observation and backscattering characteristics of the objects on earth's surface

2.3 Damage detection methodology

After coregistering the two SAR images, re-sampling was done changing the resolution from 1.25 m to 0.6 m so that it can be compared to the pan-sharpened 0.6 m QuickBird images. To remove the speckle in the SAR imagery, Lee adaptive filter [13] with a 21×21 pixel window was applied to each image. The adaptive filter produces an accurate estimate of the backscattering coefficient inside homogeneous stationary areas while preserving edge and texture therefore preferable for SAR imagery.

Then each intensity image was converted to backscatter in ground range (sigma naught, σ_0) utilizing the equation (1), (2) and (3) after Fritz [14]. Two parameters back scattering difference value (d) and correlation coefficient (r) were calculated within a 51×51 pixel window of the pre and post-event image using equations (4) and (5).

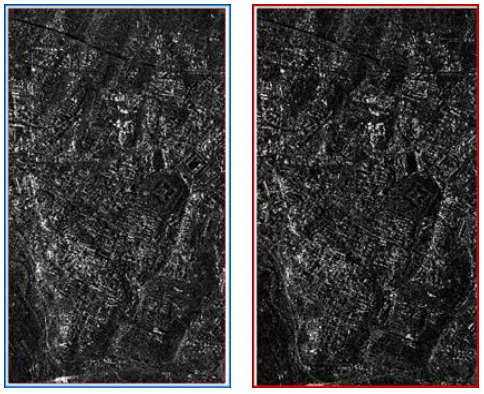

Fig.5 : Intensity images of the study area

$$\sigma_0\,(\text{db}) = \beta_0(\text{db}) + 10\log_{10}(\text{Sin}\ \theta_{\text{loc}}) \qquad (1)$$

where,

$$\beta_0(\text{db}) = 10\log_{10}(\text{Calibration factor} * \text{DN}^2) \quad (2)$$

$$\theta_{loc} = [GIM - (GIM \bmod 10)]/100 \quad (3)$$

Here β_0 refers to the backscatter per unit area in slant range and σ_0 refers to backscatter per unit area in ground range. Geocoded incidence angle mask (GIM) gives the local incidence angle and it is the angle between the radar beam and the normal to the illuminated surface. GIM mod 10 represents the remainder of the division of GIM by10. Figure 5 shows the intensity images of the study area.

$$d = \bar{I}a_i - \bar{I}b_i \quad (4)$$

$$r = \frac{N\sum_{i=1}^{N} Ia_i Ib_i - \sum_{i=1}^{N} Ia_i \sum_{i=1}^{N} Ib_i}{\sqrt{\left(N\sum_{i=1}^{N} Ia_i^{\,2} - \left(\sum_{i=1}^{N} Ia_i\right)^2\right)\cdot\left(N\sum_{i=1}^{N} Ib_i^{\,2} - \left(\sum_{i=1}^{N} Ib_i\right)^2\right)}_i} \quad (5)$$

Here, Ia_i, Ib_i represent the i-th pixel values of the post-event and pre-event images respectively and $\bar{I}a_i$, $\bar{I}b_i$ are the average values of 51×51 pixels surrounding the i-th pixel. Similarly, we also calculate normalized density vegetative index (NDVI) using equation (6) from the post event QuickBird optical image for comparison with *r* and *d*.

$$\text{NDVI} = (\text{NIR} - \text{R})/NIR + R)_i \quad (6)$$

Where, NIR and R represent digital number of a pixel in the near infrared band and the red band image respectively. NDVI ranges from -1 to +1 and gives the amount of biomass within a pixel [15].

3. Result and discussion

Figure 6 is the color composite image with a combination of post event as red while pre-event as green and blue bands. Red marks the possible change in aftermath of an earthquake. Likewise, Fig. 7 shows the correlation and back scattering difference images. Values for correlation differs from -0.5 to 1 while for the backscattering coefficient difference it is -11.4 to 12.2. The low correlation values and high back scattering may be the place for the possible damaged area. To check this one case is presented here in Fig. 8. The composite image in Fig 8(a) (Red: post event and Green, Blue: pre-event) shows some bright spot indicating the possible change. We can notice the low correlation and high back scattering in the area marked with rectangle. QuickBird image of the same area also indicates the building damage during the earthquake.

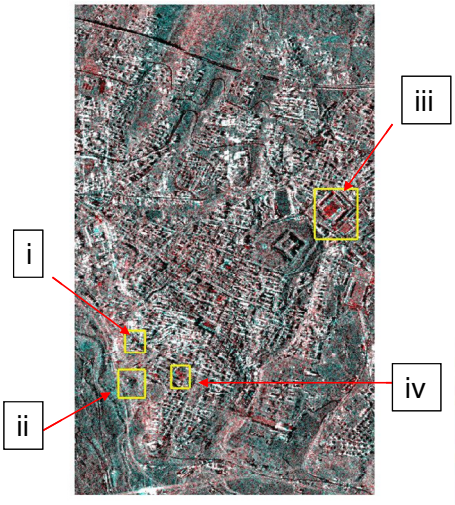

Fig. 6: RGB color composite R: post event, G, B: pre-event

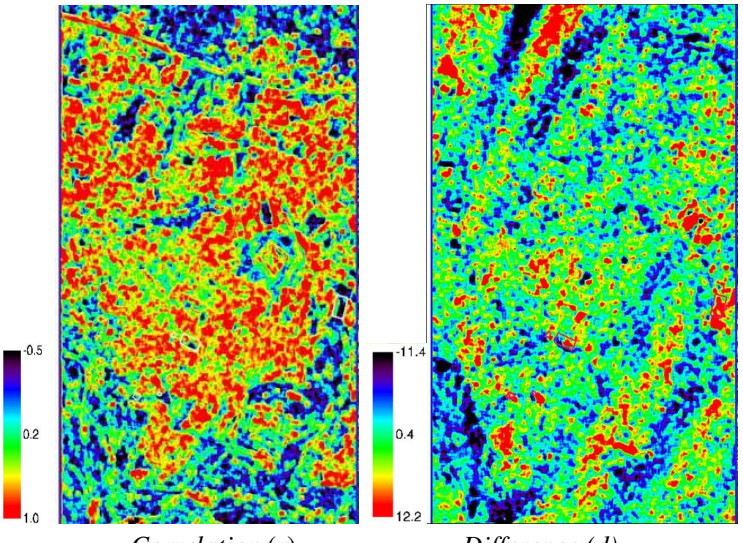

Correlation (r) *Difference (d)*

Fig. 7: Correlation and backscattering difference images

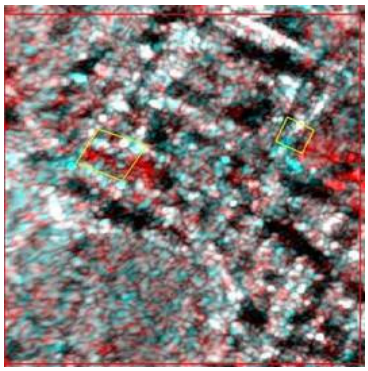

(a) Color Composite

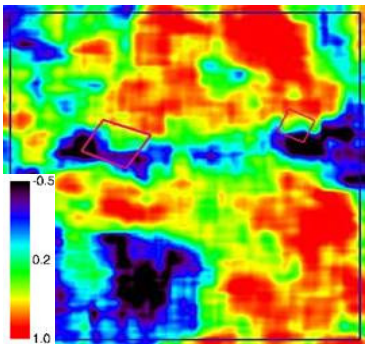

(b) Correlation

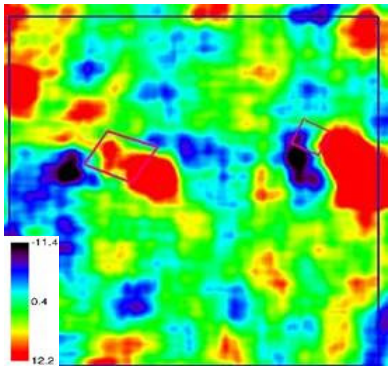

(c) Difference

(d) QuickBird (2009.4.8)

Fig. 8: Correlation and difference map of a damaged area corresponding to the area (iv) in Fig.6

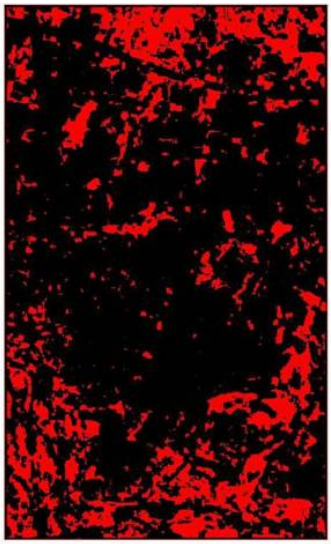

(a) SAR 2009.4.13
$r \leq 0.3$

(b) 2009.4.8
NDVI ≤ 0.16

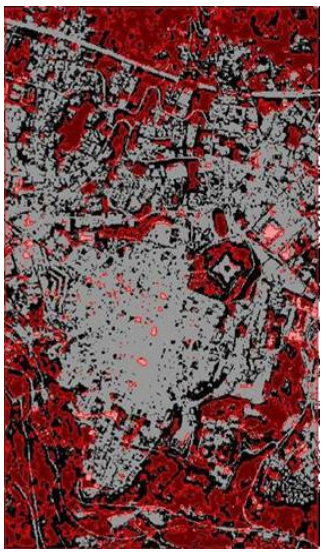

(c) Overlay of correlation over NDVI

Fig. 9: NDVI and correlation map of L'Aquila area

We also used the post event QuickBird optical image (multispectral, four bands) to calculate normalized density vegetative index (NDVI). We also prepared images from low correlation values ($r \leq 0.3$) and low NDVI values (≤ 0.16) as seen in Fig. 9(a) and 9(b).

(a) (b)

Fig. 10: Layover of intersection between low NDVI and low r over QB image (a) case in a damaged area corresponding to the area (iv) in Fig.6 (b) case in an undamaged area corresponding to the area (ii) in Fig.6

(a) (b) (c)

Fig. 11: Overlay of intersection between high d and r low NDVI over QB image. Here (a) and (b) are from the damaged areas while (c) is the parking area. Note that (a), (b) and (c) correspond to the areas (iv), (i) and (iii) respectivley, in Fig.6

When the values of low correlation ($r \leq 0.3$) were overlaid to possible damaged area (NDVI ≤ 0.16) as seen in Fig. 10, we found that building damaged area was with low NDVI and low correlation (Fig. 10(a)). However, some green areas with low NDVI are having low correlation as seen in Fig. 10 (b). From this, it can be inferred that vegetation is clearly affecting the X-band imagery. Likewise, comparison of high back scattering difference (d) with low NDVI areas are shown in Fig. 11. Damaged building was observed with low NDVI and negative high backscattering difference as in Fig. 11(a). This is obvious for the reason that once the buildings are damaged after earthquakes, the radar sensor receives less backscatter from the damaged buildings compared to the intact buildings. However, Fig. 11(b) shows damaged building with positive high backscatter. This was the case of 5-storey student dormitory building, which was totally collapsed killing eight people. This building was connected to others building but they did not suffer collapse [16]. If we see the structure layout in the area, we can see that intact buildings surround the damaged building.

When the buildings are damaged, their surface roughnesses are increased than before leading to the diffuse scattering from the damaged buildings. This causes increased response arisen from the damaged building to intact building as seen in Fig. 12 (b). This in turn might have led to the increased travel path of reflected radar signal from the damaged building causing some shift in the response from the damaged building. High backscatter of damaged buildings is also reported by other researchers [8, 11]. Vehicle parking area is also showing high backscatter as in Fig. 11 (c) and this may be caused by the vehicle parking after the earthquake event.

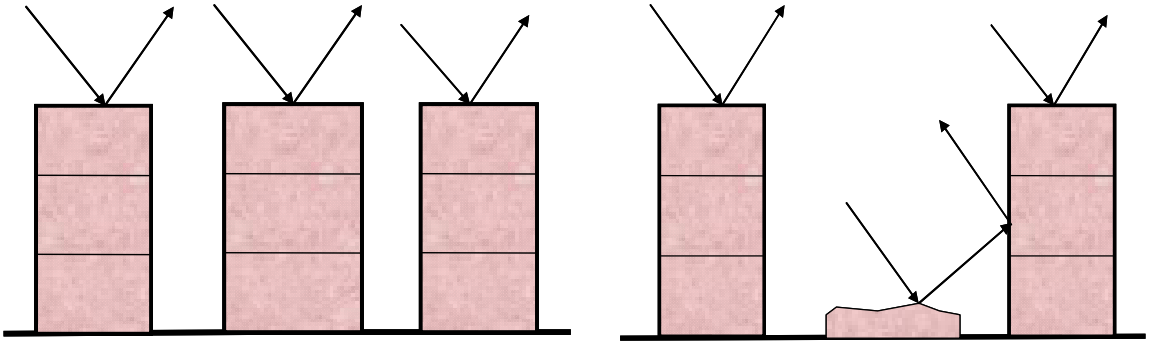

(a) (b)

Fig. 12: Schematic diagram of backscatter from (a) undamaged buildings (b) a collapsed building in close proximity to undamaged buildings

4. Conclusions

Spaceborne high-resolution SAR images are reliable and weather independent data source. With the advent of the high-resolution SAR images, new possibilities in the different fronts including damage detection in the times of emergency have evolved. We use high-resolution TerraSAR-X SAR data for the damage detection in the 2009 L'Aquila earthquake. Difference and correlation coefficient between two TerraSAR-X images taken in different time were calculated. NDVI was calculated from QuickBird image and compared with the difference and correlation coefficients from TerraSAR-X images. It was also found that X-band imagery was sensitive to the vegetation and therefore requires consideration in doing damage detection in urban areas.

Acknowledgements

The TerraSAR-X images used in this study were made available from SAR Application Research Committee, organized by PASCO Corporation, Tokyo, Japan.

References

[1] ISDR, http://www.unisdr.org/eng/library/lib-terminology-eng%20home.htm, 2010.

[2] T. LILLES., KIEFE, R., and CHIPMAN. J., 2004, *Remote Sensing and Image interpretation,* John Wiley and Sons, Inc, USA.

[3] SHINOZUKA, M., GHANEM, R., HOUSHMAD, B., and MANSOURI, S., 2000, "Damage Detection in Urban Areas by SAR Imagery", Journal of Engineering Mechanics. Vol.126 (7), pp. 769-777.

[4] MATSUOKA, M., and YAMAZAKI, F., 2004, "Use of Satellite SAR Intensity Imagery for Detecting Building Areas Damaged Due to Earthquakes", *Earthquake Spectra*, Vol.20, No. 3, pp. 975-994.

[5] STUCCHI, M., MELETTI, C., RAVIDA, A., D'AMIO., V. and CAPERA, A., 2010, "Historical earthquakes and seismic hazard of the L'Aquila area", *Progettazione Sismica*, Vol.1, No.3 pp. 23-34.

[6] United States Geological Survey,

http://earthquake.usgs.gov/earthquakes/shakemap/global/shake/2009fcaf/, 2010.

[7] CASAROTTI, C., PAVESE, A., and PALESO, S., 2010, "Seismic Response of the San Salvatore Hospital of Coppito (L'Aquila) during the Earthquake of April 6th 2009", *Progettazione Sismica*, Vol.1, No.3 pp. 159-172.

[8] BALZ, T., and LIAO, M., 2010, "Building Damage Detection Using Post-Seismic High-Resolution SAR Satellite Data", *International Journal of Remote Sensing*, 31: 13, pp. 3369 – 3391.

[9] YONEZAWA, C., and TAKEUCHI, S., 2001, "Decorrelation of SAR data by Urban Damages caused by the 1995 Hyogoken-nanbu Earthquake, " *International Journal of Remote Sensing*, Vol.22 No.3, pp. 1585-1600.

[10] MATSUOKA, M., and YAMAZAKI, F., 2005, "Building Damage mapping for the 2004 Nigata-ken Chetsu Earthquake using Radarsat Images ", *Earthquake Spectra*, Vol.21 (SI), pp. 285-294.

[11] MATSUOKA, M., YAMAZAKI, F., and H. OHKURA., 2007, "Damage Mapping for the 2004 Nigata-ken Chetsu Earthquake using Radarsat Images", *Urban Remote Sensing Joint Event, IEEE*, Paris, France, CD-ROM.

[12] STRAMONDO, S., BIGNAMI, C., CHINI, M., PIERDICCA, N., and TERTULLIANI, A., 2006, "Satellite Radar and Optical Remote Sensing for Earthquake Damage Detection: Results for Different Case Studies', *International Journal of Remote Sensing*, Vol.27 No.20, pp. 4433-4447.

[13] LEE, J. S., 1980, "Digital Image Enhancement and Noise Filtering by Use of Local Statistics", *IEEE Transaction, Pattern Analysis and Machine Intelligence, Photographic Surveying and Remote Sensing*, Vol.2, No.2, pp.165-168.

[14] TerraSAR-X Ground Segment Level 1b Product Format Specification (10.12.2007). Fritz X-GSDD-3307 Issue,1.3, 2007,[online]available; http://sss.tetrrasar-x.dlr.de.

[15] MIURA, H., and MIDORIKAWA, S., 2008, "Detection of Slope Failure Areas Using IKONOS Images and Digital Elevation Model for the 2004 Niigata-ken Chuestu, Japan Earthquake", *6th International Workshop on Remote Sensing for Disaster Applications.*

[16] Japan Association of Earthquake Engineering and Architecture Institute of Japan, 2009. "Quick Report of the JAEE/AIJ Joint Survey for the L'Aquila Italy Earthquake of April 6, 2009", http://sismo.iis.u-tokyo.ac.jp/Research.files/topic4.files/topic4-014.files/T4-14-2.pdf